Journal of Cellular Physiology

High Fluence Low-Power Laser Irradiation Induces Apoptosis via Inactivation of Akt/GSK3β Signaling Pathway

LEI HUANG, SHENGNAN WU, AND DA XING*

MOE Key Laboratory of Laser Life Science & Institute of Laser Life Science, College of Biophotonics, South China Normal University, Guangzhou 510631, China

High fluence low-power laser irradiation (HF-LPLI) is a newly discovered stimulus through generating reactive oxygen species (ROS) to trigger cell apoptosis. Activation of glycogen synthase kinase 3β (GSK3β) is proved to be involved in intrinsic apoptotic pathways under various stimuli. However, whether the proapoptotic factor GSK3β participates in HF-LPLI-induced apoptosis has not been elucidated. Therefore, in the present study, we investigated the involvement of GSK3β in apoptosis under HF-LPLI treatment (120 J/cm^2, 633 nm). We found that GSK3β activation could promote HF-LPLI-induced apoptosis, which could be prevented by lithium chloride (a selective inhibitor of GSK3β) exposure or by GSK3β-KD (a dominant-negative GSK3β) overexpression. We also found that the activation of GSK3β by HF-LPLI was due to the inactivation of protein kinase B (Akt), a widely reported and important upstream negative regulator of GSK3β, indicating the existence and inactivation of Akt/GSK3β signaling pathway. Moreover, the inactivation of Akt/GSK3β pathway depended on the fluence of HF-LPLI treatment. Furthermore, vitamin c, a ROS scavenger, completely prevented the inactivation of Akt/GSK3β pathway, indicating ROS generation was crucial for the inactivation. In addition, GSK3β promoted Bax activation by down-regulating Mcl-1 upon HF-LPLI treatment. Taken together, we have identified a new and important proapoptotic signaling pathway that is consisted of Akt/GSK3β inactivation for HF-LPLI stimulation. Our research will extend the knowledge into the biological mechanisms induced by LPLI.

J. Cell. Physiol. 226: 588–601, 2011. © 2010 Wiley-Liss, Inc.

High fluence low-power laser irradiation (HF-LPLI) can interfere with cell cycle and inhibit cell proliferation, which could be used to control certain types of hyperplasia (Gross and Jelkmann, 1990; O'Kane et al., 1994). This research is consistent with the results obtained by Zhang et al. (2008), which reveals that when light irradiation fluence exceeds 25 J/cm^2, a significant suppression of cell viability is observed in HeLa cells. Previously, we have demonstrated that HF-LPLI induces human lung adenocarcinoma (ASTC-a-1) cells apoptosis by activating caspase-3 with fluence $\geq$60 J/cm^2 (Wang et al., 2005; Wu et al., 2007). We also demonstrate that HF-LPLI (80, 120 J/cm^2) triggers cell apoptosis through mitochondrial oxidative damage indicated by the collapse of mitochondrial transmembrane potential ($\Delta\psi$m; Wu et al., 2007). Subsequently, we ascertain that HF-LPLI induces cell apoptosis via cyclosporine A-sensitive mitochondrial permeability transition, and cytotoxic doses of reactive oxygen species (ROS) generation has been demonstrated to be a determinant of cell apoptosis (Wu et al., 2009). However, the mechanism of apoptosis caused by HF-LPLI has not been fully identified.

Glycogen synthase kinase 3β (GSK3β) is a serine/threonine kinase that regulates many fundamental cellular functions including cell cycle, microtubule dynamics, protein synthesis, gene expression, and apoptosis (Grimes and Jope, 2001). GSK3β exerts its actions by directly phosphorylating various substrates including cyclin D (Diehl et al., 1998), Tau (Hanger et al., 1992), translation factor eukaryotic initiation factor 2B (Pap and Cooper, 2002), c-Jun (de Groot et al., 1993), c-Myc (He et al., 1998), and β-catenin (Ciani and Salinas, 2005). Although GSK3β is considered to be a constitutively active enzyme, its activity is tightly controlled by its phosphorylation levels. Akt activation is often effective for GSK3β inactivation by increasing the serine-9 phosphorylation (Cross et al., 1995). In addition, several other signaling pathways are also involved in the modulation of GSK3β activity, such as Wnt pathway (Frame and Cohen, 2001; Doble and Woodgett, 2003) and MAPK/p90Rsk pathway (Stambolic and Woodgett, 1994).

Accumulated evidences suggest that GSK3β is an upstream regulator of apoptosis and possesses proapoptotic characteristics. GSK3β promotes cell apoptosis caused by oxidative stress (Shin et al., 2004), DNA damage (Tan et al., 2006), endoplasmic reticulum stress (Kim et al., 2005), and ceramide (Mora et al., 2002). In addition, the catalytically inactive mutant of GSK3β or treatment with inhibitors of

Abbreviations: ASTC-a-1, human lung adenocarcinoma cells; COS-7, African green monkey SV-40-transformed kidney fibroblast cells; GSK3β, glycogen synthase kinase 3β; HepG2, human hepatocellular liver carcinoma cells; H_2DCFDA, dichlorodihydrofluorescein diacetate; HF-LPLI, high fluence low-power laser irradiation; LPLI, low-power laser irradiation; NAC, *N*-acetylcysteine; ROS, reactive oxygen species; Vc, vitamin c.

Contract grant sponsor: National Basic Research Program of China;
Contract grant number: 2010CB732602.
Contract grant sponsor: Program for Changjiang Scholars and Innovative Research Team in University;
Contract grant number: IRT0829.
Contract grant sponsor: National Natural Science Foundation of China;
Contract grant numbers: 30870676, 30870658.

*Correspondence to: Da Xing, MOE Key Laboratory of Laser Life Science & Institute of Laser Life Science, College of Biophotonics, South China Normal University, Guangzhou 510631, China.
E-mail: xingda@scnu.edu.cn

Received 30 April 2010; Accepted 27 July 2010

Published online in Wiley Online Library (wileyonlinelibrary.com), 3 August 2010.
DOI: 10.1002/jcp.22367

© 2010 WILEY-LISS, INC.

GSK3β, such as lithium chloride (LiCl), protects cells from some apoptotic stimuli (Pap and Cooper, 1998; Hetman et al., 2000). Moreover, the inhibition of GSK3β through the phosphorylation of the serine-9 can reduce apoptosis (Li et al., 2000). It has been proposed that inhibition of GSK3β by the PI3K/Akt signaling pathway may lead to the anti-apoptotic effects of Akt (Pap and Cooper, 1998; Wang et al., 2002). However, whether the proapoptotic factor GSK3β is involved in HF-LPLI-induced apoptosis has not been investigated, so it is of notable consequence to bring to light whether GSK3β is activated following HF-LPLI and, if so, how that activation is originated.

In this study, using flow cytometry, single-molecule fluorescence imaging and Western blot analysis, we examined the proapoptotic functions of GSK3β under HF-LPLI treatment and discussed the correlation mechanisms. We tried to establish the view that the inactivation of Akt/GSK3β signaling pathway played an important role on HF-LPLI-induced apoptosis. Our findings will extend the knowledge of cellular signaling mechanisms of HF-LPLI-induced apoptosis.

Materials and Methods

Cell culture

ASTC-a-1 cells, HeLa cells, human hepatocellular liver carcinoma (HepG2) cells, and African green monkey SV-40-transformed kidney fibroblast (COS-7) cells were grown on 22-mm culture glasses, in Dulbecco's modified Eagle's medium (DMEM; Life Technologies, Inc., Grand Island, NY) containing 10% fetal bovine serum (FBS; GIBCO, Co. Ltd., Grand Island, NY), 50 units/ml penicillin and 50 μg/ml streptomycin. Cells were maintained in a humidified, 37°C incubator with 5% CO_2 and 95% air.

Plasmids, reagents, and antibodies

pEYFP-GSK3β, pCGN-GSK3β-WT (wild type), and pCGN-GSK3β-KD (dominant-negative GSK3β) were kindly provided by Prof. John H. Kehrl (Shi et al., 2006) and Prof. Mien-Chie Hung (Ding et al., 2007), respectively. pDsRed-mit and pCFP-Bax were kindly provided by Prof. Yukiko Gotoh (Tsuruta et al., 2002) and Prof. Gilmore (Valentijn et al., 2003), respectively. Hemagglutinin epitope (HA)-tagged constitutively active Akt (Myr-Akt) and dominant-negative Akt (DN-Akt) were presented by Prof. Jin Q. Cheng (Yang et al., 2007).

Staurosporine (STS; 1 μM), LiCl (20 mM), hydrogen peroxide (H_2O_2; 1 mM), *N*-acetylcysteine (NAC; 5 mM) and vitamin c (Vc; 100 μM) were procured from Sigma (St. Louis, MO). Wortmannin (100 nM) was procured from BIOMOL Research Laboratories, Inc. (Plymouth, PA).

Anti-phospho-Akt (Thr308) antibody, anti-phospho-Akt (Ser473) antibody, anti-phospho-GSK3β (Ser9) antibody, anti-Akt antibody, anti-GSK3β antibody, anti-Bax antibody, and anti-caspase-3 antibody were acquired from Cell Signaling Technology (Beverly, MA). Anti-Mcl-1 antibody and anti-β-actin antibody were acquired from Santa Cruz Biotechnology (Santa Cruz, CA). Finally, HA tag antibody was obtained from Sigma.

Cell transfection and HF-LPLI treatment

Transient transfection was carried out using Lipofectamine™ 2000 (Invitrogen, Carlsbad, CA) reagent according to manufacturer's recommendations. Cells were seeded on 22-mm culture glasses or 60-mm plates 1 day prior to transfection. The total amount of plasmids for transfection was 0.5 or 5 μg. Cells were maintained in serum-free medium during transfection, and replaced with fresh culture medium 6 h later. After 24 h expression, cells were subjected to different treatments.

For irradiation of a single cell, the experiment was conducted as described in our previous work (Wu et al., 2009). Laser irradiation was performed through the objective lens (40×/NA1.45) of the inverted microscope (LSM510-ConfoCor2; Zeiss, Jena, Germany) in laser scanning mode. The cells in the selected area were irradiation for 10 min with a fluence of 120 J/cm^2. The power intensity was maintained at 0.2 W/cm^2. For irradiation of multiple cells, the cells were irradiated with a He–Ne laser (632.8 nm, HN-1000; Guangzhou, China) for 1.66, 3.33, 6.66, 10, 13.33 min in the dark with the corresponding fluence of 20, 40, 80, 120, and 160 J/cm^2, respectively. The irradiation light fluence rate was again maintained at 0.2 W/cm^2.

Flow cytometry

For FACS analysis, Annexin-V-FITC conjugate, PI dyes, and binding buffer were used as standard reagents. Flow cytometry was performed using a FACScanto II flow cytometer (Becton Dickinson, Mountain View, CA) with excitation at 488 nm. Fluorescent emission of FITC was measured at 515–545 nm and that of DNA–PI complexes at 564–606 nm. Cell debris was excluded from the analysis by an appropriate forward light scatter threshold setting. Compensation was used wherever necessary.

ROS measurements

To quantify ROS generation caused by HF-LPLI, HF-LPLI plus Vc, H_2O_2 or HF-LPLI plus H_2O_2, ASTC-a-1 cells were incubated with 10 μM H_2DCFDA (Invitrogen) for 30 min at 37°C. After incubation, cells were washed with PBS, trypsinized, and resuspended in PBS solution. DCF fluorescence (the fluorescent product of H_2DCFDA) was measured using FACScanto II flow cytometer (excitation at 488 nm, emission at 515–545 nm) and data were analyzed with CELL Quest software (Becton Dickinson).

Bax gene silencing by shRNA

RNA interference of Bax was performed using Bax-shRNA plasmid (p-Genesil-3-Bax) purchased from Genesil Biotechnology (Wuhan, China). The following sequences were targeted to silence Bax by shRNA expression: AACATGGAGCTGCAGAGGATGAdTdT. Also, p-Genesil-3 containing non-specific shRNA was used as a negative control (p-Genesil-3-con). The targeting sequences of non-specific shRNA were CTGAAGTATTCCGCGTACG. For transfection, ASTC-a-1 cells were seeded in 60-mm plates at 50% confluency, and then the cells were transfected with 2 μg p-Genesil-3-Bax and p-Genesil-3-con, respectively, using Lipofectamine™ 2000 according to Invitrogen transfection protocols. After transfection, transfected cells (colonies) were selected by culture with G418 (Sigma; for ASTC-a-1 cells, 800 μg/ml for 1 week). The efficiency of Bax-shRNA knockdown was identified by Western blot analysis.

Cell lysates collection

For Western blot analysis, cells in 60-mm plates were washed three times with phosphate-buffered saline (PBS) and were lysed with 150 μl of lysis buffer (20 mM Tris, pH 7.4, 150 mM NaCl, 2 mM EDTA, 2 mM EGTA, 1 mM sodium orthovanadate, 50 mM sodium fluoride, 1% TritonX-100, 0.1% SDS and 100 mM phenylmethylsulfonyl fluoride). For caspase-3 activity assay, cells were lysed with 150 μl lysis buffer without sodium orthovanadate. The lysates were collected in microcentrifuge tubes and centrifuged. Protein concentrations were determined using the Bradford method. The lysates were stored at −80°C for Western blot.

Western blot analysis

Cell lysates were mixed with Laemmli sample buffer (2% SDS) and placed in boiling water for 10 min. Proteins were separated in 15% SDS–polyacrylamide gels for Bax and caspase-3, and in 12% SDS–polyacrylamide gels for phospho-Thr308-Akt, phospho-Ser473-Akt, total Akt, HA-Akt, phospho-Ser9-GSK3β, total GSK3β, Mcl-1, and β-actin. The proteins were transferred to nitrocellulose membranes and incubated with primary antibodies of Bax

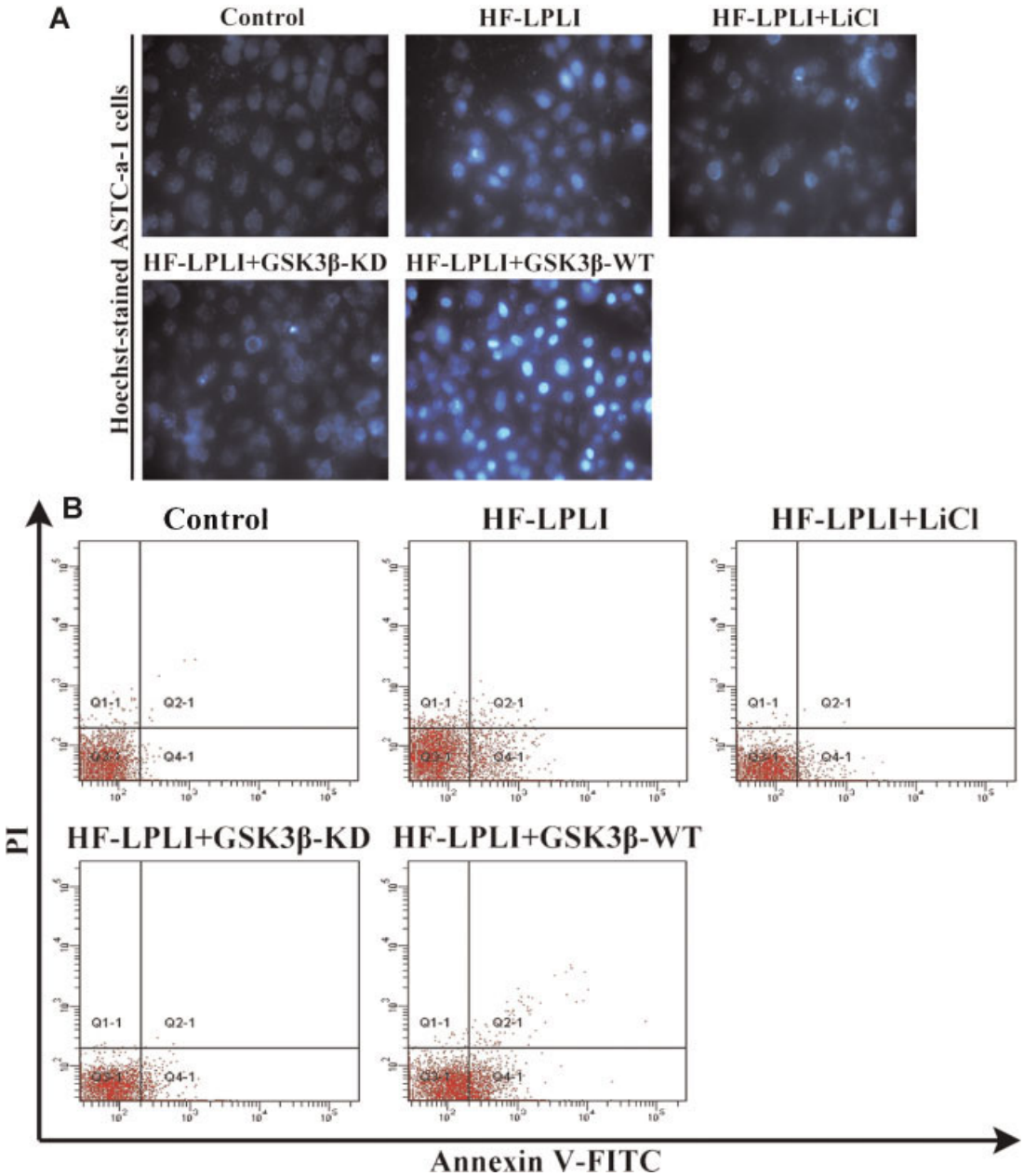

Fig. 1. GSK3β promotes cell apoptosis in response to HF-LPLI stimulation. ASTC-a-1 cells were transfected with pGSK3β-WT, pGSK3β-KD, or pre-treated with LiCl (20 mM) for 24 h. The cells were treated with HF-LPLI (120 J/cm^2) except for control group. A: Representative sequential images of apoptotic morphology of treated cells were observed with Hoechst 33258 staining. The cells were photographed at 40× magnifications. Data represent mean ± SEM (n = 3). B,C: Cell death analysis of treated cells was performed by flow cytometry with annexin V/PI double staining. Representative images and quantitative analysis were shown in (B) and (C), respectively. Data represent mean ± SEM (n = 3; $^*P < 0.05$ vs. control cells, $^\#P < 0.05$ vs. indicated cells). D: Representative Western blot analysis of treated cells was performed to detect protein levels of full length caspase-3 and cleaved caspase-3. E: Quantitative analysis of cleaved caspase-3 protein levels in treated cells. Data represent mean ± SEM (n = 3; $^*P < 0.05$ vs. control cells, $^\#P < 0.05$ vs. indicated cells). [Color figure can be viewed in the online issue, which is available at wileyonlinelibrary.com.]

(1:1,000), caspase-3 (1:1,000), phospho-Thr308-Akt (1:1,000), phospho-Ser473-Akt (1:1,000), total Akt (1:1,000), HA (1:1,000), phospho-Ser9-GSK3β (1:1,000), total GSK3β (1:1,000), Mcl-1 (1:500) or β-actin (1:1,000). Bax, Caspase-3, phospho-Ser473-Akt, total Akt, HA-Akt, phospho-Ser9-GSK3β, and total GSK3β were labeled with goat anti-rabbit conjugated to IRDyeTM 800 secondary antibodies (Rockland Immunochemicals, Gilbertsville, PA). Phospho-Thr308-Akt, Mcl-1, and β-actin were labeled with goat anti-mouse conjugated to Alexa Flour 680 secondary antibodies (Invitrogen). Detection was performed using the LI-COR Odyssey Scanning Infrared Fluorescence Imaging System (LI-COR, Inc., Lincoln, NE).

Immunofluorescence

For Bax activation, ASTC-a-1 cells cultured on glass cover slips were stained with Mito-Tracker Deeper 633 Red (100 nM; Molecular Probes, Inc.) at 37°C for 30 min. Then the cells were fixed with 4% paraformaldehyde for 10 min, followed by permeabilization in 0.5% CHAPS for 30 min. The cells were

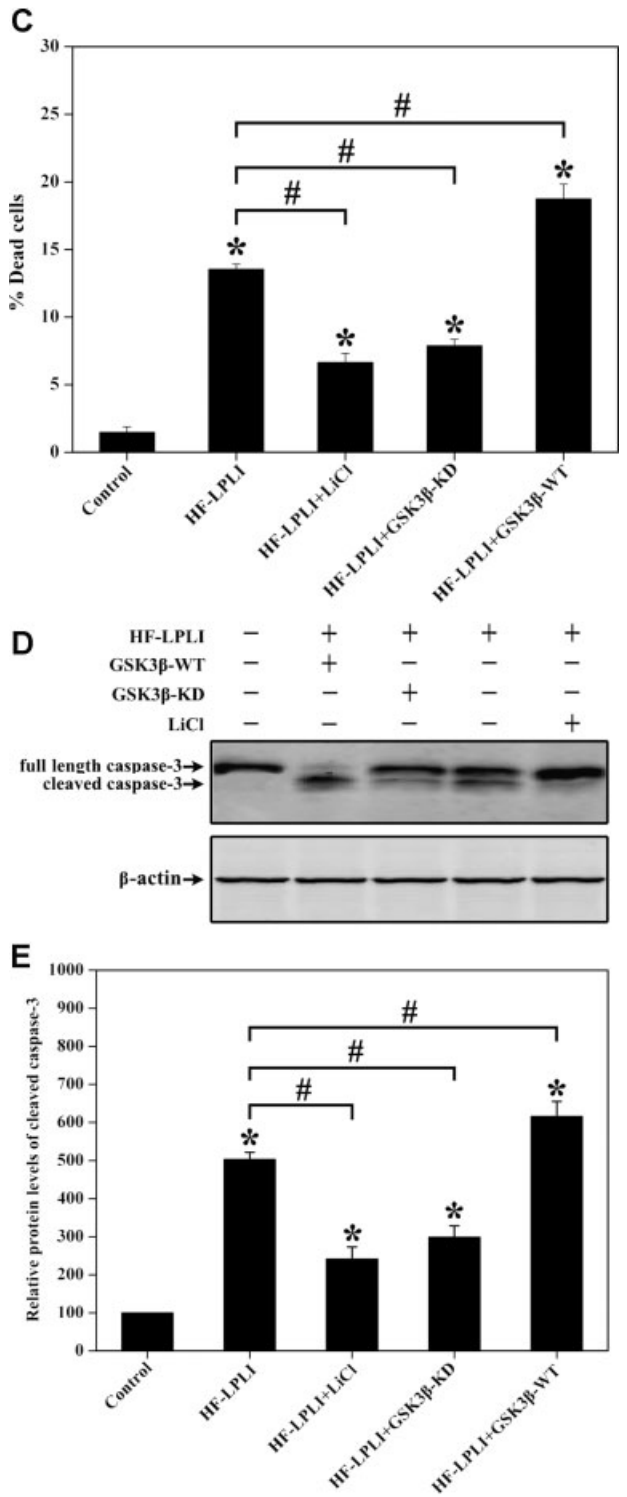

Fig. 1. (*Continued*)

incubated in blocking buffer (10% bovine serum albumin in PBS) for 1 h at room temperature, followed by incubation with anti-Bax antibody 6A7 (diluted 1:30 in blocking buffer; Abcam, Cambridge, United Kingdom) at 4°C overnight. Samples were washed three times for 5 min in PBS, and then incubated for 1 h with Alexa Fluor 488-conjugated goat anti-mouse secondary antibody (diluted 1:300 in blocking buffer; Invitrogen) at room temperature. Images were acquired using a confocal microscope through a 40× oil objective (LSM510-ConfoCor2; Zeiss).

Statistical analysis

MATLAB software was used for data analysis. For fluorescence emission intensity analysis, a background subtraction was performed for the data. For the analysis of Bax translocation, images were analyzed with MATLAB 6.5 software by drawing regions around individual cells and then computing standard deviations of the intensity of the pixels (punctate/diffuse) and integrated brightness (total brightness; Munoz-Pinedo et al., 2006).

All assays were repeated independently for a minimum of three times. Data are represented as mean ± SEM. Statistical analysis was performed with Student's paired *t*-test. Differences were considered statistically significant at $P < 0.05$.

Results

GSK3β promotes cell apoptosis induced by HF-LPLI

Nuclear staining by Hoechst 33258 dyes was used to monitor the morphological changes of the nucleus in cells under different treatments. Nuclear condensation and cell shrinkage revealed the characteristic morphology associated with apoptosis. ASTC-a-1 cells were divided into five groups. Two of the five groups with GSK3β-WT and GSK3β-KD overexpression, respectively, were treated with HF-LPLI. Another group was incubated with GSK3β inhibitor LiCl for 24 h before HF-LPLI treatment. Cells without any treatment were set as control. The last one of the five groups was treated with HF-LPLI alone. Cells were stained with Hoechst 33258 dyes 4 h post HF-LPLI treatment and then monitored by confocal microscopy. The representative fluorescence images of cells labeled with Hoechst 33258 under various treatments were shown in Figure 1A. The results revealed that all the HF-LPLI-treated cells under different conditions displayed obvious nuclear condensation and chromatin fragmentation, confirming the occurrence of cell apoptosis in comparison with control cells. The details were as follows: GSK3β-WT overexpression resulted in higher levels of cell apoptosis than HF-LPLI treatment alone. In contrast, GSK3β-KD overexpression resulted in lower levels of cell apoptosis than HF-LPLI treatment alone. Besides, LiCl exposure resulted in similar levels of cell apoptosis with the condition of GSK3β-KD overexpression. Quantitative analysis (Fig. 1B,C) of cell death rate by flow cytometry revealed that all the HF-LPLI-treated cells under different conditions showed cell death in comparison with control cells. Specifically, GSK3β-WT overexpression resulted in higher rates of cell death than HF-LPLI treatment alone. In contrast, GSK3β-KD overexpression resulted in lower rates of cell death than HF-LPLI treatment alone. Besides, LiCl exposure resulted in similar rates of cell death with the condition of GSK3β-KD overexpression. These results demonstrate that GSK3β promotes cell apoptosis induced by HF-LPLI.

Subsequently, activity of caspase-3 under different treatments was examined with Western blot analysis (Fig. 1D). Our results showed that cleaved caspase-3 was detected in all cells treated with HF-LPLI in comparison with the control cells. For the details, GSK3β-WT overexpression resulted in higher levels of cleaved caspase-3 than HF-LPLI treatment alone (Fig. 1E). In contrast, cells with GSK3β-KD overexpression resulted in similar levels of cleaved caspase-3 with LiCl exposure. Both GSK3β-KD overexpression and LiCl exposure resulted in lower levels of cleaved caspase-3 than HF-LPLI treatment alone. The results shown in Figure 1D,E demonstrate that GSK3β promotes cell apoptosis (indicated by the enhanced activity of caspase-3) induced by HF-LPLI.

HF-LPLI induces GSK3β nuclear translocation

A powerful method for imaging and quantifying the spatio-temporal nuclear translocation of GSK3β in living cells is the transfection of cells with YFP-GSK3β reporter. To assess the effect of HF-LPLI on GSK3β nuclear translocation, YFP-GSK3β reporter was transfected into ASTC-a-1 cells and COS-7 cells, and the dynamic changes of YFP-GSK3β was monitored in real-time in living cells under different treatments by confocal microscope. The results showed that HF-LPLI (120 J/cm^2) caused a marked 2.4-fold within 8 h increase in YFP-GSK3β nuclear fluorescence emission intensities, compared to that in the control cells (Fig. 2A,B), revealing the nuclear translocation of GSK3β. The phenomenon of GSK3β nuclear translocation is consistent with that caused by STS or wortmannin treatment, the conditions known to inactivate Akt, indicating the possibility of Akt involves in GSK3β activation under HF-LPLI treatment. Similar results were observed in COS-7 cells (Fig. 2C,D).

HF-LPLI induces GSK3β activation through Akt inactivation

We next investigated whether GSK3β activation could be reliably initiated by Akt inactivation under HF-LPLI treatment. Phosphorylation levels of Akt and GSK3β in ASTC-a-1 cells under HF-LPLI (120 J/cm^2) treatment were identified with Western blot analysis. Date shown in Figure 3A–C revealed that HF-LPLI caused significant reduction of the levels of phospho-Thr308-Akt, phospho-Ser473-Akt, and phospho-Ser9-GSK3β, which were positively correlated with irradiation time, whereas total levels of Akt and GSK3β were unchanged. STS and wortmannin were set as positive controls. Wortmannin reduced both the levels of phospho-Thr308-Akt and phospho-Ser473-Akt, while STS only reduced the levels of phospho-Thr308-Akt. Experiments performed in both HeLa cells and HepG2 cells yielded similar results that HF-LPLI reduced the levels of phospho-Thr308-Akt, phospho-Ser473-Akt, and phospho-Ser9-GSK3β (Fig. 3D–F). These results demonstrate that HF-LPLI causes significant inactivation of Akt and activation of GSK3β indicated by the decrease in phosphorylation levels, suggesting that HF-LPLI induces inactivation of the Akt/GSK3β signaling pathway.

In order to further confirm the result that HF-LPLI caused GSK3β activation through Akt inactivation, the ASTC-a-1 cells were divided into five groups. Two of the five groups with Myr-Akt and DN-Akt overexpression, respectively, were treated with HF-LPLI (120 J/cm^2). Another group was treated with wortmannin alone. Cells without any treatment were set as control. The last group was treated with HF-LPLI alone. Changes in the levels of phospho-Ser9-GSK3β and the exogenous expression of Myr-Akt and DN-Akt were detected using Western blot analysis 4 h post HF-LPLI treatment. The results revealed that overexpression of Myr-Akt resulted in higher levels of phospho-Ser9-GSK3β than HF-LPLI treatment alone (Fig. 3G,H). In contrast, overexpression of DN-Akt

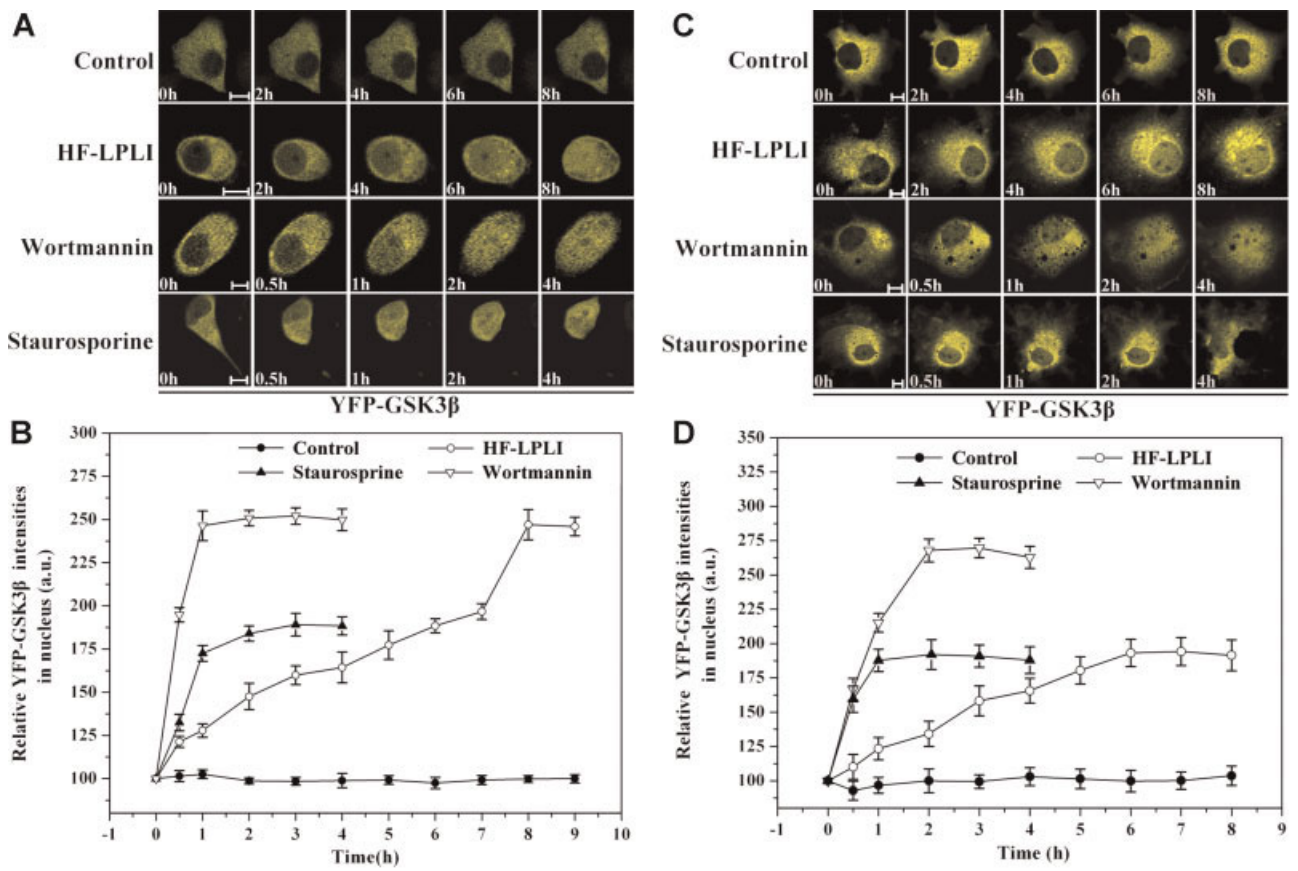

Fig. 2. HF-LPLI induces GSK3β nuclear translocation. A,C: Representative sequential images of ASTC-a-1 cells (A) and COS-7 cells (C) expressing YFP-GSK3β (yellow emission) was in response to different treatments; Bar = 10 μm. B,D: Quantitative analysis of relative YFP-GSK3β fluorescence emission intensities of nucleus in ASTC-a-1 cells (B) and in COS-7 cells (D) was subjected to different treatments. Data represent mean ± SEM (n = 5). [Color figure can be viewed in the online issue, which is available at wileyonlinelibrary.com.]

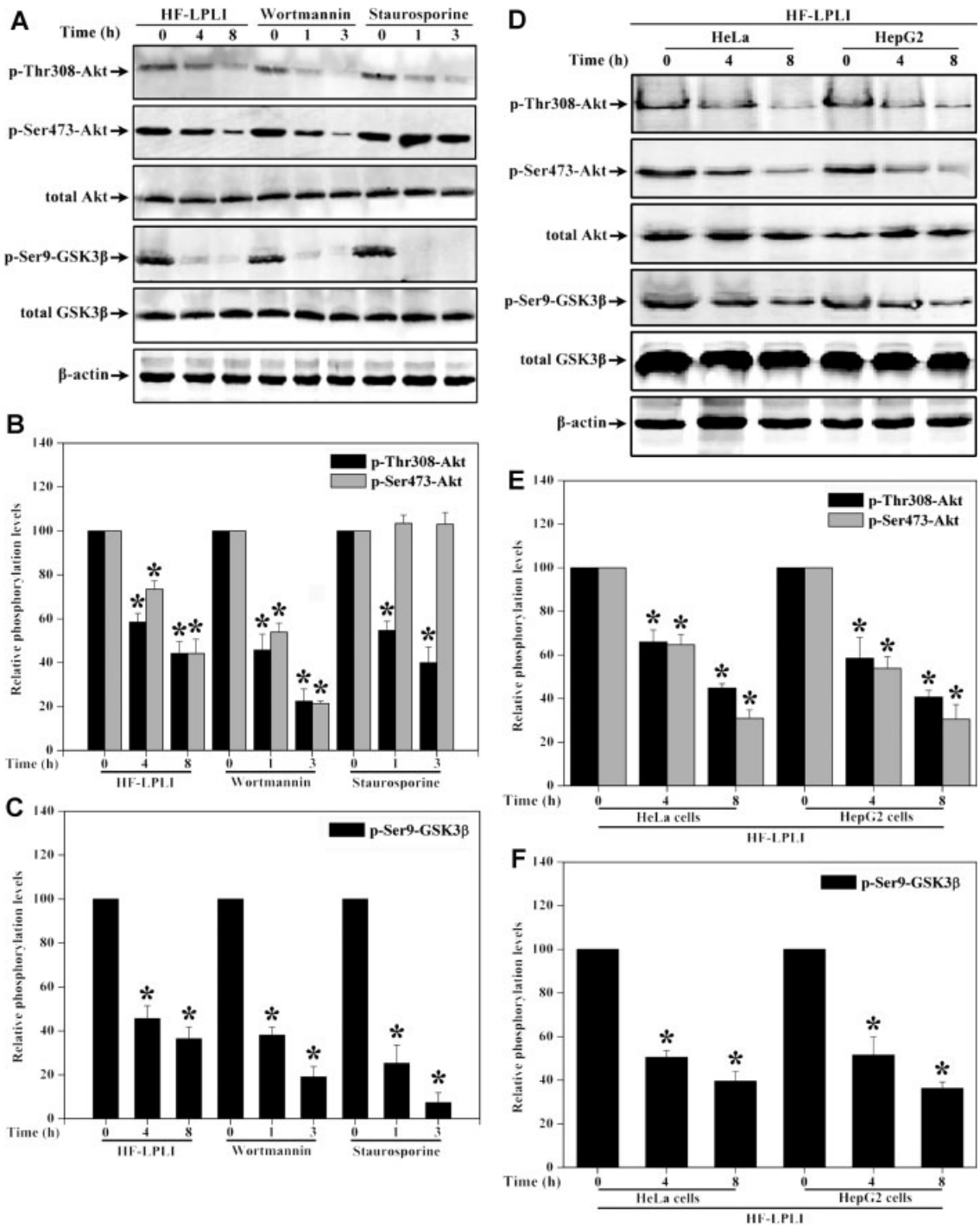

Fig. 3. HF-LPLI induces activation of GSK3β through inactivation of Akt. A: Western blot analysis of ASTC-a-1 cells received different treatments was performed to detect phospho-Thr308-Akt, phospho-Ser473-Akt, phospho-Ser9-GSK3β, total Akt, and total GSK3β. Data were the representative graph. B,C: Quantitative analysis of the levels of phospho-Thr308-Akt, phospho-Ser473-Akt, and phospho-Ser9-GSK3β in ASTC-a-1 cells received different treatments. Data represent mean ± SEM (n = 3; *P < 0.05 vs. 0 h). D: Western blot analysis of HeLa cells and HepG2 cells treated with HF-LPLI (120 J/cm^2) was performed to detect phospho-Thr308-Akt, phospho-Ser473-Akt, phospho-Ser9-GSK3β, total Akt, and total GSK3β. Data were the representative graph. E,F: Quantitative analysis of the levels of phospho-Thr308-Akt, phospho-Ser473-Akt, and phospho-Ser9-GSK3β in HeLa cells and HepG2 cells treated with HF-LPLI (120 J/cm^2). Data represent mean ± SEM (n = 3; *P < 0.05 vs. 0 h). G: ASTC-a-1 cells expressing Myr-Akt or DN-Akt were treated with HF-LPLI (120 J/cm^2). Cells without any treatment were set as control. Wortmannin was used as a positive control. The graph was representative Western blot analysis of phospho-Ser9-GSK3β in cells received different treatments. H: Quantitative analysis of the levels of phospho-Ser9-GSK3β in ASTC-a-1 cells received different treatments. Data represent mean ± SEM (n = 3; *P < 0.05 vs. indicated cells). I: Representative fluorescence images of ASTC-a-1 cells expressing YFP-GSK3β (yellow emission) in response to different treatments; Bar = 50 μm. J: The percentages of ASTC-a-1 cells with YFP-GSK3β nuclear translocation in response to different treatments. Data represent mean ± SEM of five independent experiments with 500 cells per conditions (*P < 0.05 vs. indicated cells). K: Exogenous expression of Myr-Akt and DN-Akt in ASTC-a-1 cells were detected using Western blot analysis. [Color figure can be viewed in the online issue, which is available at wileyonlinelibrary.com.]

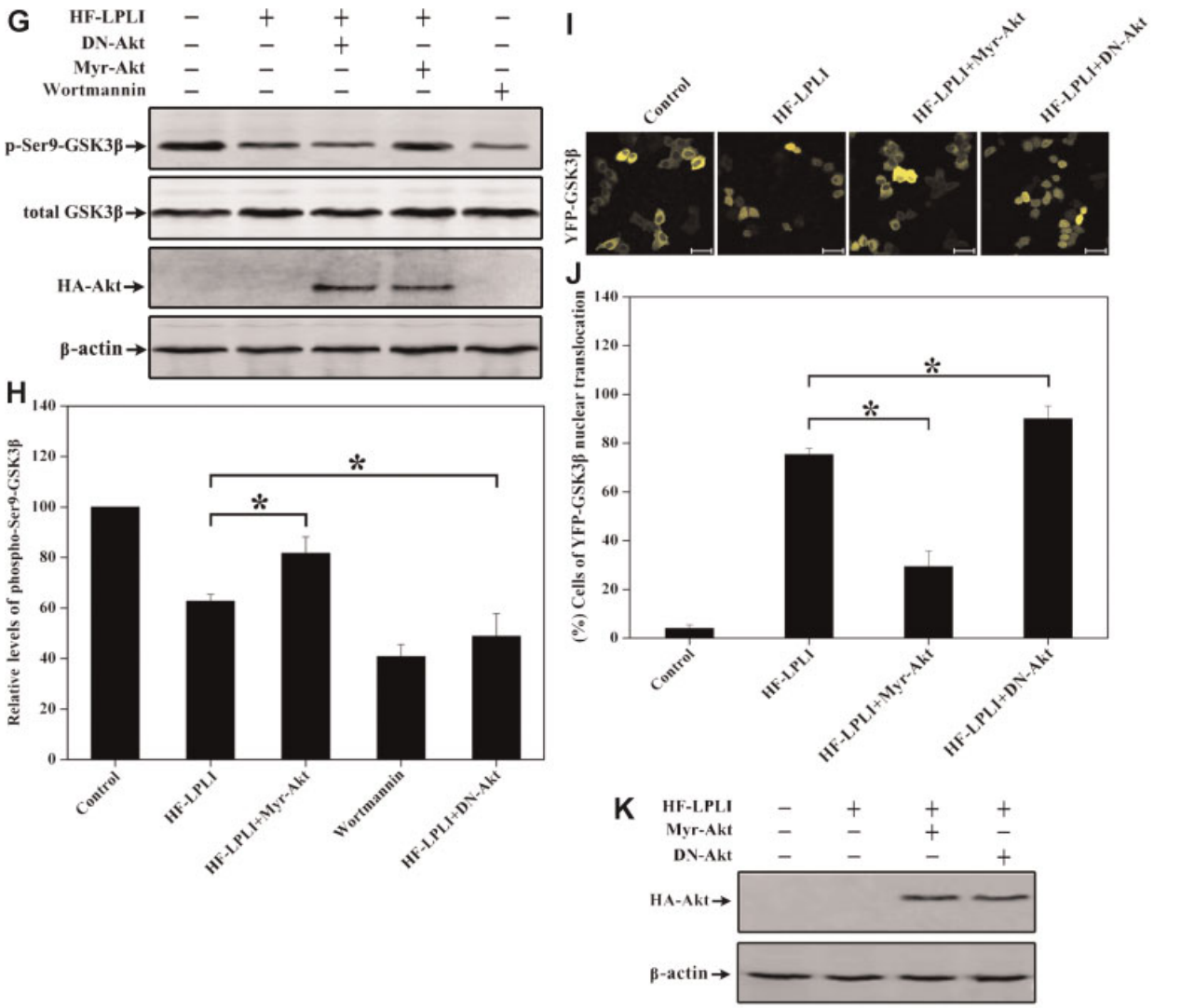

Fig. 3. (*Continued*)

resulted in lower levels of phospho-Ser9-GSK3β than HF-LPLI treatment alone. Wortmannin was set as a positive control to decrease the levels of phospho-Thr308-Akt and phospho-Ser473-Akt. These results confirm that HF-LPLI causes GSK3β activation through Akt inactivation.

We also explored whether Akt had effect on GSK3β nuclear translocation induced by HF-LPLI. To this end, YFP-GSK3β was co-expressed with Myr-Akt or DN-Akt in ASTC-a-1 cells and then the cells were treated with HF-LPLI (120 J/cm^2). Cells expressing YFP-GSK3β alone without any treatment were set as control. The representative fluorescence images of YFP-GSK3β nuclear translocation in cells under HF-LPLI treatment were shown in Figure 3I, and the quantitative analysis of YFP-GSK3β nuclear translocation was shown in Figure 3J. Exogenous expression of Myr-Akt and DN-Akt were identified using Western blot analysis (Fig. 3K). We found that Myr-Akt overexpression resulted in lower percentages of YFP-GSK3β nuclear translocation than HF-LPLI treatment alone. In contrast, DN-Akt overexpression resulted in higher percentages of YFP-GSK3β nuclear translocation than HF-LPLI treatment alone. There was little YFP-GSK3β nuclear translocation in control cells. These results suggest that Akt regulates GSK3β nuclear translocation in response to HF-LPLI stimulation.

HF-LPLI induces inactivation of the Akt/GSK3β signaling pathway in a dose-dependent manner

Next, changes in the activities of Akt and GSK3β under different fluences of HF-LPLI treatment were investigated in ASTC-a-1 cells. The phosphorylation levels of Akt and GSK3β were examined with Western blot analysis 4 h post HF-LPLI treatment at the fluence of 20–160 J/cm^2. Concomitant with the increase of HF-LPLI fluence, the levels of phospho-Thr308-Akt, phospho-Ser473-Akt, and phospho-Ser9-GSK3β were decreased whereas the total levels of Akt and GSK3β were unchanged (Fig. 4A–C). These results demonstrate that HF-LPLI induces inactivation of the Akt/GSK3β signaling pathway in a dose-dependent manner.

ROS mediates inactivation of the Akt/GSK3β signaling pathway under HF-LPLI treatment

To examine whether ROS contributed to the activation of GSK3β during HF-LPLI-induced apoptosis, ASTC-a-1 cells

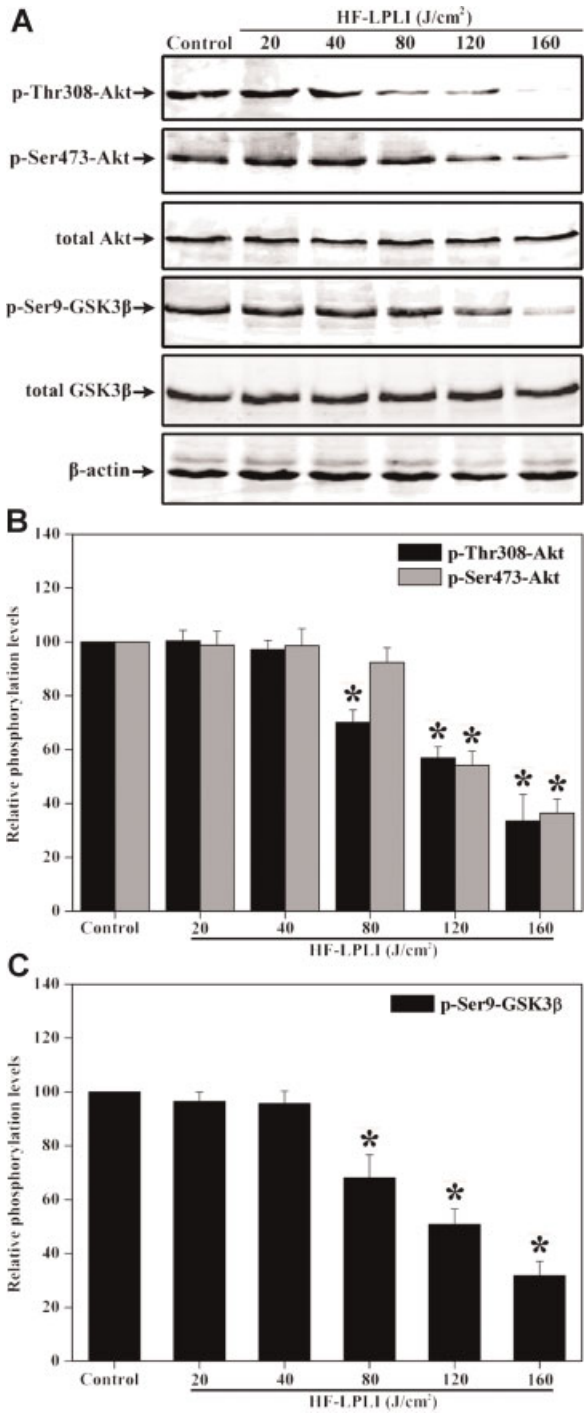

Fig. 4. HF-LPLI induces inactivation of Akt/GSK3β signaling pathway in a dose-dependent manner. A: ASTC-a-1 cells were treated with HF-LPLI at the fluence of 20, 40, 80, 120, or 160 J/cm^2. After 4 h, the levels of phospho-Thr308-Akt, phospho-Ser473-Akt, phospho-Ser9-GSK3β, total Akt, and total GSK3β were detected with Western blot analysis. Data were the representative graph. B,C: Quantitative analysis of the levels of phospho-Thr308-Akt, phospho-Ser473-Akt, and phospho-Ser9-GSK3β in ASTC-a-1 cells received HF-LPLI treatment at different fluences. Data represent mean ± SEM (n = 3; $^*P < 0.05$ vs. control cells).

were transfected with YFP-GSK3β and the dynamic changes of YFP-GSK3β were monitored under various treatments. The representative fluorescence images of YFP-GSK3β in cells under different treatments were shown in Figure 5A, and the quantitative analysis of YFP-GSK3β fluorescence emission intensities of nucleus was shown in Figure 5B. Intracellular ROS generation was quantified by DCF fluorescence under various treatments (Fig. 4D). Our experiments revealed that nuclear translocation of YFP-GSK3β under HF-LPLI (120 J/cm^2) treatment was slower than that under combined treatments of HF-LPLI and H_2O_2 (Fig. 5A,B). In marked contrast, Vc or NAC, ROS scavenger, significantly decreased HF-LPLI-induced translocation of YFP-GSK3β. In addition, the percentages of cells with YFP-GSK3β nuclear translocation 4 h after each treatment were calculated as follows (n = 5, 500 cells per condition): HF-LPLI caused 81% translocation; H_2O_2 caused 86% translocation; HF-LPLI combined with H_2O_2 caused 98% translocation; HF-LPLI combined with Vc or NAC caused 15% and 29% translocation, respectively, suggesting ROS generation was involved in the activation of GSK3β.

In order to explore whether ROS mediated activation of GSK3β through inactivation of Akt under HF-LPLI treatment, the phosphorylation levels of Akt and GSK3β under different treatments were detected with Western blot analysis. As shown in Figure 5E–G, the phosphorylation levels of Akt and GSK3β under HF-LPLI (120 J/cm^2) treatment were higher than that under combined treatments of HF-LPLI and H_2O_2. In contrast, the levels under HF-LPLI treatment were lower than those under HF-LPLI treatment in the presence of Vc. The total levels of Akt and GSK3β were unchanged. These results demonstrate that HF-LPLI induces inactivation of the Akt/GSK3β pathway mediated by ROS generation.

GSK3β promotes Bax activation through down-regulation of Mcl-1 under HF-LPLI treatment

To understand the effects of GSK3β on Bax activation under HF-LPLI treatment, ASTC-a-1 cells co-expressing CFP-Bax, YFP-GSK3β, and DsRed-mit were treated with HF-LPLI (120 J/cm^2). Fluorescence images and quantitative analysis of fluorescence emission intensities of CFP-Bax and YFP-GSK3β revealed that nuclear translocation of GSK3β occurred prior to mitochondrial translocation of Bax under HF-LPLI treatment in comparison with control cells (Fig. 6A–D), suggesting that GSK3β could promote Bax activation.

To confirm the result that GSK3β promoted Bax activation under HF-LPLI treatment, immunofluorescence technology was used to detect Bax activation with Bax 6A7 antibody with or without LiCl exposure or overexpression of GSK3β-KD. Figure 6E showed that HF-LPLI induced high levels of activated Bax compared with the control cells 8 h post-treatment. Conversely, LiCl pre-treatment or overexpression of GSK3β-KD significantly suppressed Bax activation. These results indicate that GSK3β activation is an upstream event of Bax activation under HF-LPLI treatment.

We also explored whether HF-LPLI-induced cell apoptosis was neutralized by Bax knockdown. ASTC-a-1 cells were transfected with Bax-shRNA. G418-resistant cells were collected, and loss of Bax was identified by Western blot analysis (Fig. 6F). As seen in Figure 6G, cell apoptosis analyzed using flow cytometry revealed that HF-LPLI resulted in obvious apoptosis compared with control cells. Knockdown of Bax by shRNA significantly suppressed HF-LPLI-induced cell apoptosis, indicating that Bax activation play an important role in the apoptotic process.

We next examined whether Mcl-1, an anti-apoptotic member of Bcl-2 family and a known substrate of GSK3β, was involved in the regulation of Bax activation under HF-LPLI

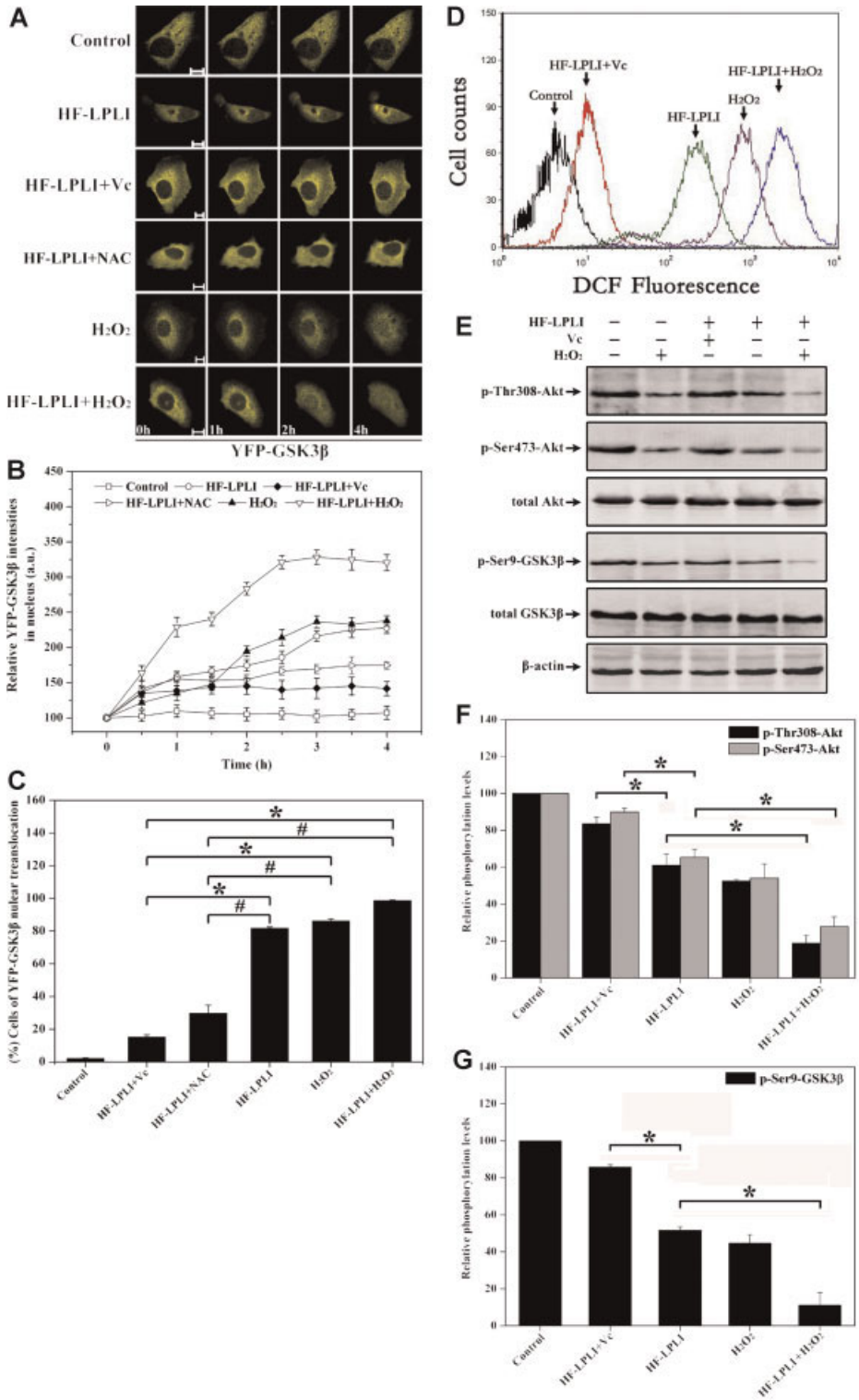

Fig. 5. ROS mediates inactivation of Akt/GSK3β signaling pathway under HF-LPLI treatment. A: Representative sequential images of ASTC-a-1 cells expressing YFP-GSK3β (yellow emission) received different treatments. Bar = 10 μm. B: Quantitative analysis of relative YFP-GSK3β fluorescence emission intensities of nucleus in ASTC-a-1 cells received different treatments. Data represent mean ± SEM (n = 5). C: The percentages of ASTC-a-1 cells with YFP-GSK3β nuclear translocation received different treatments. Data represent mean ± SEM of five independent experiments with 500 cells per conditions ($^{*}P < 0.05$ vs. indicated cells, $^{\#}P < 0.05$ vs. indicated cells). GSK3β nuclear translocation was regulated by ROS generation under HF-LPLI treatment. D: ASTC-a-1 cells were incubated with 10 μM H_2DCFDA for 30 min at 37°C and then treated with HF-LPLI, HF-LPLI plus Vc, H_2O_2 or HF-LPLI plus H_2O_2. ROS generation was determined by DCF fluorescence and measured using FACS analysis. E–G: Representative Western blot analysis (E) and quantitative analysis (F,G) for the levels of phospho-Thr308-Akt, phospho-Ser473-Akt, and phospho-Ser9-GSK3β in ASTC-a-1 cells received different treatments. Data represent mean ± SEM (n = 3; $^{*}P < 0.05$ vs. indicated cells; Vc, Vitamin c; NAC, *N*-acetylcysteine). [Color figure can be viewed in the online issue, which is available at wileyonlinelibrary.com.]

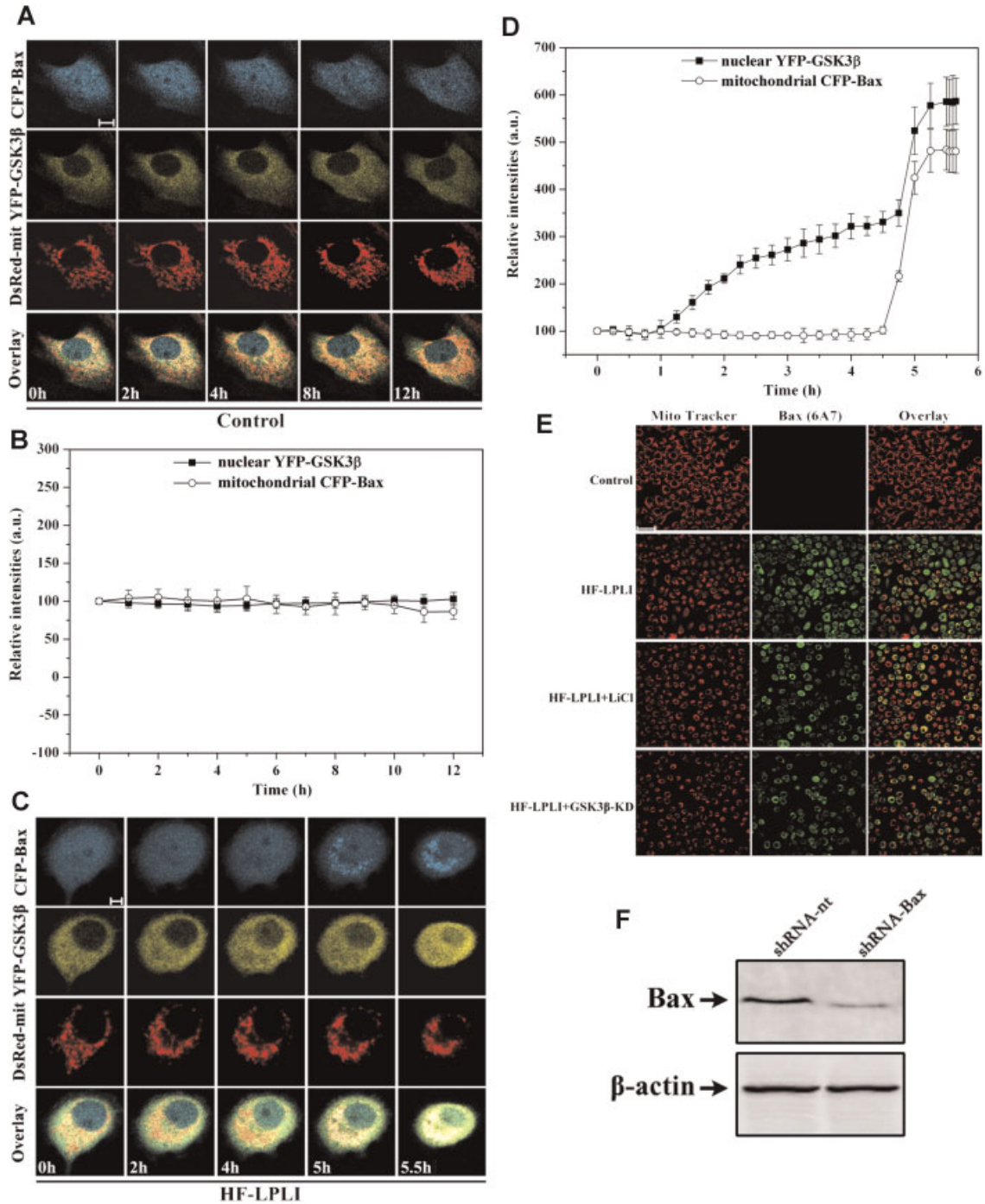

Fig. 6. GSK3β promotes Bax activation through down-regulation of Mcl-1 under HF-LPLI treatment. A,C: Representative sequential images of ASTC-a-1 cells co-expressing CFP-Bax (cyan emission), YFP-GSK3β (yellow emission), and DsRed-mit (red emission) without any treatment (A) or treated with HF-LPLI (120 J/cm^2) (C). Bar = 10 μm. B,D: Quantitative analysis of relative nuclear YFP-GSK3β and mitochondrial CFP-Bax fluorescence emission intensities in ASTC-a-1 cells without any treatment (B) or treated with HF-LPLI (120 J/cm^2) (D). Data shown in B and D represent mean ± SEM (n = 5). E: Immunofluorescence analysis of Bax activation under HF-LPLI treatment (120 J/cm^2) with or without LiCl (20 mM 24 h) exposure or overexpression of GSK3β-KD. Cells without any treatment were set as control. Cells were fixed and immunostained with Bax 6A7 antibody to determine the localization of activated Bax (green emission). Mitochondria were labeled with MitoTracker Deeper Red 633 (red emission). Bar = 50 μm (n = 3). F: ASTC-a-1 cells were transfected with either specific Bax shRNA (shRNA-Bax) or non-targeting shRNA (shRNA-nt) using Lipofectamine™ 2000. G418-resistant cells were collected, and Bax protein expression was identified by Western blot analysis. G: The ASTC-a-1 cells stably transfected with shRNA-Bax were treated with HF-LPLI (120 J/cm^2), and then apoptosis of treated cells was performed by flow cytometry with annexin V staining 8 h post-treatment (n = 3). H,I: Representative Western blot analysis (H) and quantitative analysis (I) for the levels of phospho-Ser9-GSK3β and Mcl-1 in ASTC-a-1 cells under HF-LPLI treatment (120 J/cm^2) with or without LiCl (20 mM 24 h) exposure. Data shown in I represent mean ± SEM (n = 3; $^*P < 0.05$ vs. indicated cells). J,K: Representative Western Blot analysis (J) and quantitative analysis (K) for the levels of Mcl-1 in ASTC-a-1 cells under HF-LPLI treatment (120 J/cm^2) with overexpression of GSK3β-WT and GSK3β-KD, respectively. Data shown in K represent mean ± SEM (n = 3; $^*P < 0.05$ vs. indicated cells). [Color figure can be viewed in the online issue, which is available at wileyonlinelibrary.com.]

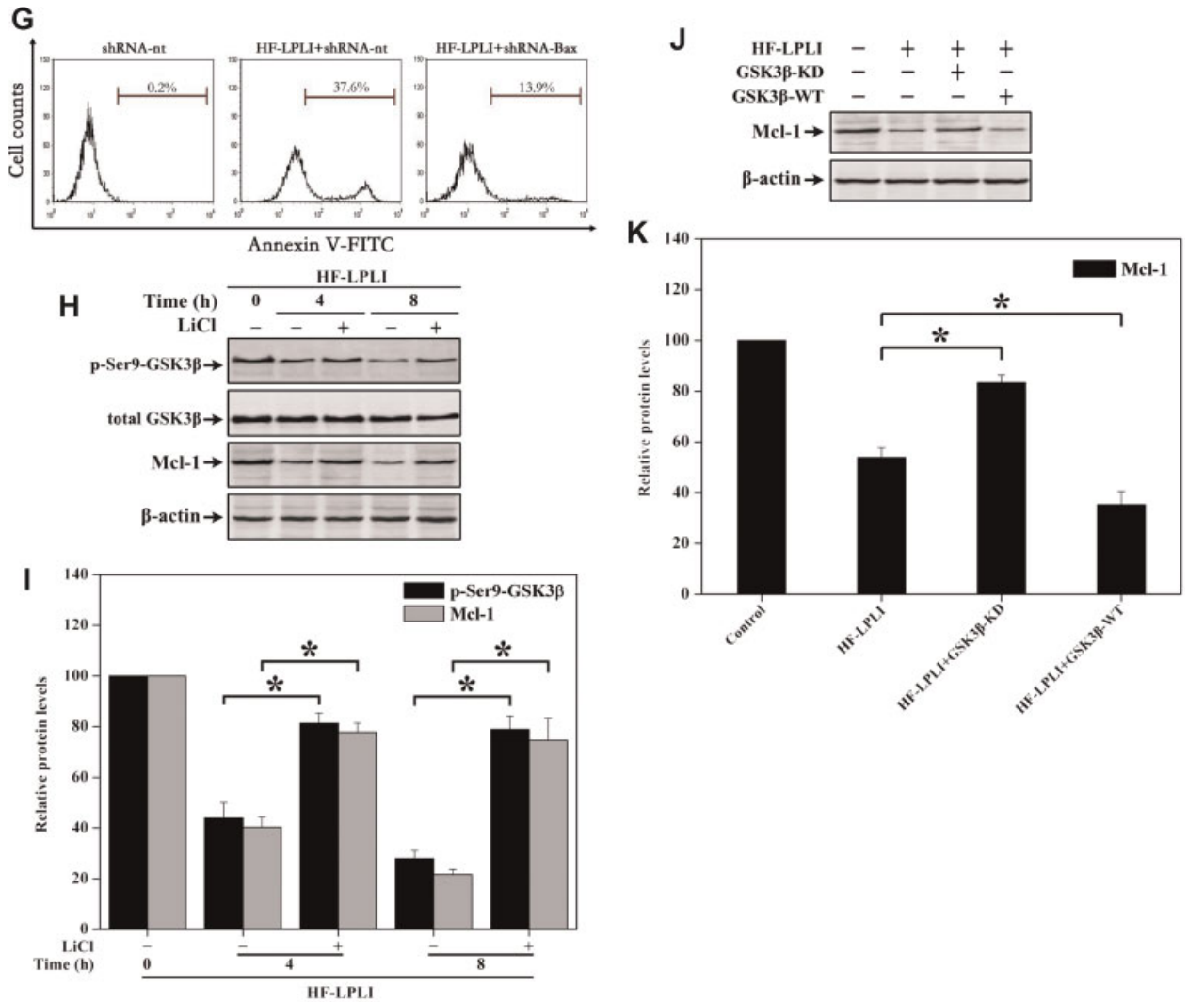

Fig. 6. (*Continued*)

treatment. ASTC-a-1 cells were treated with HF-LPLI with or without LiCl exposure. Western blot analysis revealed that down-regulation of Mcl-1 protein levels was concomitant with decrease of phospho-Ser9-GSK3β levels in response to HF-LPLI (Fig. 6H and I), which were both prevented by LiCl. To further investigate the contribution made by GSK3β to down-regulation of Mcl-1, GSK3β-WT, and GSK3β-KD were transfected into ASTC-a-1 cells, and the protein levels of Mcl-1 were evaluated using Western blot analysis. As seen in Figure 6J,K, under HF-LPLI treatment, Mcl-1 protein levels were lower in cells overexpressing GSK3β-WT than that in non-overexpressing cells. In contrast, the levels were higher in cells overexpressing GSK3β-KD than that in non-overexpressing cells, suggesting that GSK3β down-regulated the protein levels of Mcl-1 in response to HF-LPLI. Taken together, results shown in Figure 6 demonstrate that GSK3β promotes Bax activation through down-regulation of Mcl-1 during HF-LPLI-induced apoptosis.

Discussion

In light of our recent report that HF-LPLI induces intrinsic pathway through mitochondrial oxidative damage, cytochrome *c* release, and caspase-3 activation, in the present study, we identified a novel signaling pathway: HF-LPLI resulted in inactivation of the Akt/GSK3β signaling pathway through ROS generation. We also demonstrated that inactivation of the Akt/GSK3β pathway could promote HF-LPLI-induced apoptosis by accelerating Bax activation.

GSK3β is tightly regulated by intracellular signaling systems when cells undergo apoptosis in response to various stimuli. Our results revealed obvious involvement of GSK3β in cell apoptosis induced by HF-LPLI. Five demonstrative evidences could support the view: (1) GSK3β promoted cell apoptosis under HF-LPLI treatment (Fig. 1); (2) HF-LPLI induced GSK3β activation and nuclear translocation through Akt inactivation (Figs. 2 and 3); (3) Inactivation of Akt/GSK3β signaling pathway triggered by HF-LPLI was dependent on the fluence of HF-LPLI treatment (Fig. 4); (4) ROS generation was crucial for inactivation of the Akt/GSK3β pathway (Fig. 5); (5) GSK3β promoted Bax activation by down-regulating Mcl-1 in response to HF-LPLI treatment (Fig. 6).

It is reported that overexpression of modest levels of GSK3β in SH-SY5Y neuroblastoma cells facilitates STS- and heat shock-induced apoptosis, and this facilitation was attenuated by treatment with LiCl (Bijur et al., 2000). Using three different

methods, we investigated the proapoptotic functions of GSK3β upon HF-LPLI treatment. Firstly, nuclear condensation and chromatin fragmentation were clearly revealed by Hoechst 33258 staining in GSK3β overexpressed cells. In addition, flow cytometry, a powerful technique for quantitative analysis, supported the view that GSK3β promoted HF-LPLI-induced apoptosis. Finally, Western blot analysis demonstrated that GSK3β promoted apoptosis by accelerating caspase-3 activation, suggesting that GSK3β activation was an upstream event of HF-LPLI-induced apoptosis. Besides, inhibition of GSK3β activation by LiCl exposure or GSK3β-KD overexpression suppressed HF-LPLI-induced apoptosis, also demonstrated the proapoptotic function of GSK3β upon HF-LPLI treatment.

Apoptotic stimuli including STS and growth factor withdrawal can cause activation and nuclear accumulation of GSK3β (Bijur and Jope, 2001), which is regulated by intracellular signaling cascades. Nuclear accumulation facilitates interaction of GSK3β with the substrates in the nucleus. Using live-cell in situ fluorescent imaging and Western blot analysis, nuclear translocation of GSK3β, and decrease of phosphorylation levels of GSK3β were observed, adequately confirming the activation of GSK3β under HF-LPLI treatment. Akt is an important upstream negative regulator of GSK3β. Our experiments corroborated that Akt was involved in the activation of GSK3β, which was evidenced by simultaneous decrease in the levels of phospho-Thr308-Akt, phospho-Ser473-Akt, and phospho-Ser9-GSK3β. In addition, DN-Akt and Myr-Akt overexpression could promote and inhibit GSK3β activity, respectively. Thus, we concluded that inactivation of the Akt/GSK3β signaling pathway was existed in HF-LPLI-induced apoptosis.

ROS play critical roles in the regulation of apoptosis (Simon et al., 2000; Chen et al., 2003). Previously, we have reported that the generation of cytotoxic ROS is crucial for HF-LPLI-induced apoptosis (Wu et al., 2009). However, whether ROS participate in the inactivation of Akt/GSK3β signaling pathway upon HF-LPLI treatment is unclear. In the present study, Vc, a ROS scavenger, completely suppressed the inactivation of Akt/GSK3β pathway under HF-LPLI treatment (Fig. 5), indicating the involvement of ROS in the pathway. Early reports reveal that the formation of ceramide is a key event in oxidative stress-induced apoptosis (Goldkorn et al., 1998; Bezombes et al., 2001). Moreover, ceramide can activate PP2A (Dobrowsky et al., 1993; Chalfant et al., 1999; Ruvolo et al., 1999), a protein phosphatase, which can inactivate Akt (Yamada et al., 2001; Li et al., 2003) and thus activate GSK3β (Ivaska et al., 2002; Lin et al., 2007). In addition, our early works show that HF-LPLI activates caspase-3 (Wang et al., 2005; Wu et al., 2007). Previous study reports that Akt is a substrate of caspase-3 and can be cleaved by caspase-3 (Martin et al., 2002). However, in our experiments, we did not detect Akt cleavage product in response to HF-LPLI stimulation (Figs. 3–5), suggesting HF-LPLI-induced Akt/GSK3β singling pathway inactivation is in a caspase-3-independent manner. Therefore, we prefer that the HF-LPLI/ROS/ceramide/PP2A signaling pathway mediates inactivation of the Akt/GSK3β signaling pathway.

The activity state of Akt/GSK3β signaling pathway can be modulated by the changes of intracellular oxidant levels upon different stimuli. Karu (1989) have reported that LPLI can through activating endogenous photoacceptors and generating ROS to modulate various biological processes. Our earlier study shows that the level of ROS generation is positive correlation with the fluence of LPLI (Zhang et al., 2008). Zhang et al. (2009) have reported that LPLI at low fluence of 0.2–1.2 J/cm^2 promotes cell proliferation through activation of PI3K/Akt signaling pathway. They also demonstrate that the activation of Akt/GSK3β pathway results in obvious attenuation of STS-induced cell apoptosis (Zhang et al., 2010). In contrast, in the present study, we showed that LPLI at high fluence (120 J/cm^2) resulted in inactivation of the Akt/GSK3β pathway and thus accelerating cell apoptosis. It was reported that lethal levels of ROS as a proapoptotic stimulus could activate PP2A (Goldbaum and Richter-Landsberg, 2002; Cicchillitti et al., 2003), whereas the sublethal levels of ROS as a physiological regulator could suppress PP2A (Whisler et al., 1995; Rao and Clayton, 2002). Besides, PP2A could dephosphorylate Akt and cause Akt inactivation (Sato et al., 2000; Beaulieu et al., 2005; Gao et al., 2005). In addition, a recent study demonstrated that H_2O_2 inhibited the phosphorylation of PDK1 and Akt in a concentration- and time-dependent manner in both PC12 cells and neuronal cells (Chen et al., 2010). These studies well supported the view that the level of ROS generation was very important for the activation of Akt/GSK3β signaling pathway. Another factor for the changes of the state of Akt/GSK3β signaling pathway lied in the different cell types. For example, Ushio-Fukai et al. (1999) has reported that H_2O_2 (200 μM) mediates Akt activation and GSK3β inactivation in vascular smooth muscle cells. In contrast, Nair and Olanow (2008) has reported that H_2O_2 (200 μM) causes Akt inactivation and GSK3β activation in PC12 cells. Shin et al. (2006) has demonstrated that H_2O_2 (500 μM) inhibits Akt and activates GSK3β in NIH3T3 cells.

GSK3β is most widely reported to be involved in the mitochondria-mediated intrinsic apoptotic pathway. Our results showed that GSK3β could promote Bax activation (Fig. 6), indicating the participation of GSK3β in the intrinsic pathway under HF-LPLI treatment. Linseman et al. (2004) have reported that GSK3β directly phosphorylates Bax and promotes its mitochondrial localization during neuronal apoptosis. On the other hand, Hongisto et al. (2008) reports that the locus of GSK3β action is downstream of *bim* gene expression where GSK3β activity governs Bim protein levels rather than direct phosphorylation Bax. Recent study shows that GSK3β can phosphorylate Mcl-1 and then leads to Mcl-1 degradation mediated by E3 ligase β-TrCP (Ding et al., 2007). Our results confirmed that GSK3β promoted Bax activation

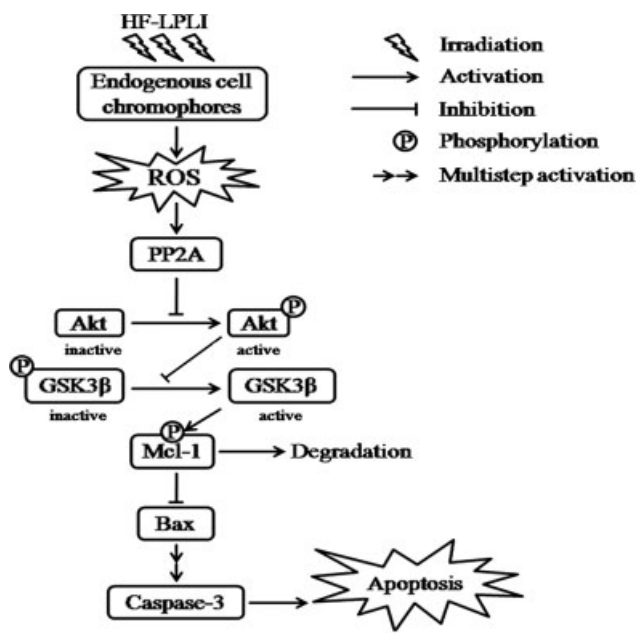

Fig. 7. A model of Akt/GSK3β signaling pathway inactivation induced by HF-LPLI.

through down-regulation of Mcl-1 during HF-LPLI-induced apoptosis because LiCl exposure or GSK3β-KD overexpression significantly suppressed down-regulation of Mcl-1 and Bax activation under these conditions (Fig. 6).

In conclusion, for the first time, we demonstrated that HF-LPLI could cause Akt/GSK3β signaling pathway inactivation through ROS generation (Fig. 7). The inactivation of the Akt/GSK3β pathway was crucial for cell apoptosis induced by HF-LPLI. We also demonstrated that GSK3β promoted Bax activation through down-regulation of Mcl-1, which provided a direct linkage between GSK3β and intrinsic apoptotic cascades during HF-LPLI-induced apoptosis. Our research provided a new proapoptotic signaling pathway under HF-LPLI treatment.

Acknowledgments

We thank Prof. John H. Kehrl (Laboratory of Immunoregulation, National Institute of Allergy and Infectious Diseases, National Institutes of Health) and Prof. Mien-Chie Hung (Department of Molecular and Cellular Oncology, The University of Texas M.D. Anderson Cancer Center) for kindly providing pEYFP-GSK3*β*, pCGN-GSK3*β*-WT, and pCGN-GSK3*β*-KD, respectively; Prof. Yukiko Gotoh (the Institute of Molecular and Cellular Bioscience, University of Tokyo), and Prof. Gilmore (The School of Biological Sciences, University of Manchester) for kindly providing pDsRed-mit and pCFP-Bax, respectively. We also thank Prof. Jin Q. Cheng (Department of Pathology and Cell Biology and Molecular Oncology Program, H. Lee Moffitt Cancer Center and College of Medicine, University of South Florida) for gifting HA-Myr-Akt and HA-DN-Akt. This work was supported by National Basic Research Program of China (2010CB732602), the Program for Changjiang Scholars and Innovative Research Team in University (IRT0829), and National Natural Science Foundation of China (30870676; 30870658).

Literature Cited

Beaulieu JM, Sotnikova TD, Marion S, Lefkowitz RJ, Gainetdinov RR, Caron MG. 2005. An Akt/beta-arrestin 2/PP2A signaling complex mediates dopaminergic neurotransmission and behavior. Cell 122:261–273.

Bezombes C, Plo I, Mansat-De Mas V, Quillet-Mary A, Negre-Salvayre A, Laurent G, Jaffrezou JP. 2001. Oxidative stress-induced activation of Lyn recruits sphingomyelinase and is requisite for its stimulation by Ara-C. FASEB J 15:1583–1585.

Bijur GN, Jope RS. 2001. Proapoptotic stimuli induce nuclear accumulation of glycogen synthase kinase-3 beta. J Biol Chem 276:37436–37442.

Bijur GN, De Sarno P, Jope RS. 2000. Glycogen synthase kinase-3beta facilitates staurosporine- and heat shock-induced apoptosis. Protection by lithium. J Biol Chem 275:7583–7590.

Chalfant CE, Kishikawa K, Mumby MC, Kamibayashi C, Bielawska A, Hannun YA. 1999. Long chain ceramides activate protein phosphatase-1 and protein phosphatase-2A. Activation is stereospecific and regulated by phosphatidic acid. J Biol Chem 274:20313–20317.

Chen Q, Chai YC, Mazumder S, Jiang C, Macklis RM, Chisolm GM, Almasan A. 2003. The late increase in intracellular free radical oxygen species during apoptosis is associated with cytochrome c release, caspase activation, and mitochondrial dysfunction. Cell Death Differ 10:323–334.

Chen L, Xu B, Liu L, Luo Y, Yin J, Zhou H, Chen W, Shen T, Han X, Huang S. 2010. Hydrogen peroxide inhibits mTOR signaling by activation of AMPKalpha leading to apoptosis of neuronal cells. Lab Invest 90:762–773.

Ciani L, Salinas PC. 2005. WNTs in the vertebrate nervous system: From patterning to neuronal connectivity. Nat Rev Neurosci 6:351–362.

Cicchillitti L, Fasanaro P, Biglioli P, Capogrossi MC, Martelli F. 2003. Oxidative stress induces protein phosphatase 2A-dependent dephosphorylation of the pocket proteins pRb, p107, and p130. J Biol Chem 278:19509–19517.

Cross DA, Alessi DR, Cohen P, Andjelkovich M, Hemmings BA. 1995. Inhibition of glycogen synthase kinase-3 by insulin mediated by protein kinase B. Nature 378:785–789.

de Groot RP, Auwerx J, Bourouis M, Sassone-Corsi P. 1993. Negative regulation of Jun/AP-1: Conserved function of glycogen synthase kinase 3 and the Drosophila kinase shaggy. Oncogene 8:841–847.

Diehl JA, Cheng M, Roussel MF, Sherr CJ. 1998. Glycogen synthase kinase-3beta regulates cyclin D1 proteolysis and subcellular localization. Genes Dev 12:3499–3511.

Ding Q, He X, Hsu JM, Xia W, Chen CT, Li LY, Lee DF, Liu JC, Zhong Q, Wang X, Hung MC. 2007. Degradation of Mcl-1 by beta-TrCP mediates glycogen synthase kinase 3-induced tumor suppression and chemosensitization. Mol Cell Biol 27:4006–4017.

Doble BW, Woodgett JR. 2003. GSK-3: Tricks of the trade for a multi-tasking kinase. J Cell Sci 116:1175–1186.

Dobrowsky RT, Kamibayashi C, Mumby MC, Hannun YA. 1993. Ceramide activates heterotrimeric protein phosphatase 2A. J Biol Chem 268:15523–15530.

Frame S, Cohen P. 2001. GSK3 takes centre stage more than 20 years after its discovery. Biochem J 359:1–16.

Gao T, Furnari F, Newton AC. 2005. PHLPP: A phosphatase that directly dephosphorylates Akt, promotes apoptosis, and suppresses tumor growth. Mol Cell 18:13–24.

Goldbaum O, Richter-Landsberg C. 2002. Activation of PP2A-like phosphatase and modulation of tau phosphorylation accompany stress-induced apoptosis in cultured oligodendrocytes. Glia 40:271–282.

Goldkorn T, Balaban N, Shannon M, Chea V, Matsukuma K, Gilchrist D, Wang H, Chan C. 1998. H_2O_2 acts on cellular membranes to generate ceramide signaling and initiate apoptosis in tracheobronchial epithelial cells. J Cell Sci 111:3209–3220.

Grimes CA, Jope RS. 2001. The multifaceted roles of glycogen synthase kinase 3beta in cellular signaling. Prog Neurobiol 65:391–426.

Gross AJ, Jelkmann W. 1990. Helium-neon laser irradiation inhibits the growth of kidney epithelial cells in culture. Lasers Surg Med 10:40–44.

Hanger DP, Hughes K, Woodgett JR, Brion JP, Anderton BH. 1992. Glycogen synthase kinase-3 induces Alzheimer's disease-like phosphorylation of tau: Generation of paired helical filament epitopes and neuronal localisation of the kinase. Neurosci Lett 147:58–62.

He TC, Sparks AB, Rago C, Hermeking H, Zawel L, da Costa LT, Morin PJ, Vogelstein B, Kinzler KW. 1998. Identification of c-MYC as a target of the APC pathway. Science 281:1509–1512.

Hetman M, Cavanaugh JE, Kimelman D, Xia Z. 2000. Role of glycogen synthase kinase-3beta in neuronal apoptosis induced by trophic withdrawal. J Neurosci 20:2567–2574.

Hongisto V, Vainio JC, Thompson R, Courtney MJ, Coffey ET. 2008. The Wnt pool of glycogen synthase kinase 3beta is critical for trophic-deprivation-induced neuronal death. Mol Cell Biol 28:1515–1527.

Ivaska J, Nissinen L, Immonen N, Eriksson JE, Kahari VM, Heino J. 2002. Integrin alpha 2 beta 1 promotes activation of protein phosphatase 2A and dephosphorylation of Akt and glycogen synthase kinase 3 beta. Mol Cell Biol 22:1352–1359.

Karu T. 1989. Photobiology of low-power laser effects. Health Phys 56:691–704.

Kim AJ, Shi Y, Austin RC, Werstuck GH. 2005. Valproate protects cells from ER stress-induced lipid accumulation and apoptosis by inhibiting glycogen synthase kinase-3. J Cell Sci 118:89–99.

Li M, Wang X, Meintzer MK, Laessig T, Birnbaum MJ, Heidenreich KA. 2000. Cyclic AMP promotes neuronal survival by phosphorylation of glycogen synthase kinase 3beta. Mol Cell Biol 20:9356–9363.

Li L, Ren CH, Tahir SA, Ren C, Thompson TC. 2003. Caveolin-1 maintains activated Akt in prostate cancer cells through scaffolding domain binding site interactions with and inhibition of serine/threonine protein phosphatases PP1 and PP2A. Mol Cell Biol 23:9389–9404.

Lin CF, Chen CL, Chiang CW, Jan MS, Huang WC, Lin YS. 2007. GSK-3beta acts downstream of PP2A and the PI 3-kinase-Akt pathway, and upstream of caspase-2 in ceramide-induced mitochondrial apoptosis. J Cell Sci 120:2935–2943.

Linseman DA, Butts BD, Precht TA, Phelps RA, Le SS, Laessig TA, Bouchard RJ, Florez-McClure ML, Heidenreich KA. 2004. Glycogen synthase kinase-3beta phosphorylates Bax and promotes its mitochondrial localization during neuronal apoptosis. J Neurosci 24:9993–10002.

Martin D, Salinas M, Fujita N, Tsuruo T, Cuadrado A. 2002. Ceramide and reactive oxygen species generated by H_2O_2 induce caspase-3-independent degradation of Akt/protein kinase B. J Biol Chem 277:42943–42952.

Mora A, Sabio G, Risco AM, Cuenda A, Alonso JC, Soler G, Centeno F. 2002. Lithium blocks the PKB and GSK3 dephosphorylation induced by ceramide through protein phosphatase-2A. Cell Signal 14:557–562.

Munoz-Pinedo C, Guio-Carrion A, Goldstein JC, Fitzgerald P, Newmeyer DD, Green DR. 2006. Different mitochondrial intermembrane space proteins are released during apoptosis in a manner that is coordinately initiated but can vary in duration. Proc Natl Acad Sci USA 103:11573–11578.

Nair VD, Olanow CW. 2008. Differential modulation of Akt/glycogen synthase kinase-3beta pathway regulates apoptotic and cytoprotective signaling responses. J Biol Chem 283:15469–15478.

O'Kane S, Shields TD, Gilmore WS, Allen JM. 1994. Low intensity laser irradiation inhibits tritiated thymidine incorporation in the hemopoietic cell lines HL-60 and U937. Lasers Surg Med 14:34–39.

Pap M, Cooper GM. 1998. Role of glycogen synthase kinase-3 in the phosphatidylinositol 3-kinase/Akt cell survival pathway. J Biol Chem 273:19929–19932.

Pap M, Cooper GM. 2002. Role of translation initiation factor 2B in control of cell survival by the phosphatidylinositol 3-kinase/Akt/glycogen synthase kinase 3beta signaling pathway. Mol Cell Biol 22:578–586.

Rao RK, Clayton LW. 2002. Regulation of protein phosphatase 2A by hydrogen peroxide and glutathionylation. Biochem Biophys Res Commun 293:610–616.

Ruvolo PP, Deng X, Ito T, Carr BK, May WS. 1999. Ceramide induces Bcl2 dephosphorylation via a mechanism involving mitochondrial PP2A. J Biol Chem 274:20296–20300.

Sato S, Fujita N, Tsuruo T. 2000. Modulation of Akt kinase activity by binding to Hsp90. Proc Natl Acad Sci USA 97:10832–10837.

Shi CS, Huang NN, Harrison K, Han SB, Kehrl JH. 2006. The mitogen-activated protein kinase kinase kinase GCKR positively regulates canonical and noncanonical Wnt signaling in B lymphocytes. Mol Cell Biol 26:6511–6521.

Shin SY, Kim CG, Jho EH, Rho MS, Kim YS, Kim YH, Lee YH. 2004. Hydrogen peroxide negatively modulates Wnt signaling through downregulation of beta-catenin. Cancer Lett 212:225–231.

Shin SY, Chin BR, Lee YH, Kim JH. 2006. Involvement of glycogen synthase kinase-3beta in hydrogen peroxide-induced suppression of Tcf/Lef-dependent transcriptional activity. Cell Signal 18:601–607.

Simon HU, Haj-Yehia A, Levi-Schaffer F. 2000. Role of reactive oxygen species (ROS) in apoptosis induction. Apoptosis 5:415–418.

Stambolic V, Woodgett JR. 1994. Mitogen inactivation of glycogen synthase kinase-3 beta in intact cells via serine 9 phosphorylation. Biochem J 303:701–704.

Tan J, Geng L, Yazlovitskaya EM, Hallahan DE. 2006. Protein kinase B/Akt-dependent phosphorylation of glycogen synthase kinase-3beta in irradiated vascular endothelium. Cancer Res 66:2320–2327.

Tsuruta F, Masuyama N, Gotoh Y. 2002. The phosphatidylinositol 3-kinase (PI3K)-Akt pathway suppresses Bax translocation to mitochondria. J Biol Chem 277:14040–14047.

Ushio-Fukai M, Alexander RW, Akers M, Yin Q, Fujio Y, Walsh K, Griendling KK. 1999. Reactive oxygen species mediate the activation of Akt/protein kinase B by angiotensin II in vascular smooth muscle cells. J Biol Chem 274:22699–22704.

Valentijn AJ, Metcalfe AD, Kott J, Streuli CH, Gilmore AP. 2003. Spatial and temporal changes in Bax subcellular localization during anoikis. J Cell Biol 162:599–612.

Wang Q, Wang X, Hernandez A, Hellmich MR, Gatalica Z, Evers BM. 2002. Regulation of TRAIL expression by the phosphatidylinositol 3-kinase/Akt/GSK-3 pathway in human colon cancer cells. J Biol Chem 277:36602–36610.

Wang F, Chen TS, Xing D, Wang JJ, Wu YX. 2005. Measuring dynamics of caspase-3 activity in living cells using FRET technique during apoptosis induced by high fluence low-power laser irradiation. Lasers Surg Med 36:2–7.

Whisler RL, Goyette MA, Grants IS, Newhouse YG. 1995. Sublethal levels of oxidant stress stimulate multiple serine/threonine kinases and suppress protein phosphatases in Jurkat T cells. Arch Biochem Biophys 319:23–35.
Wu S, Xing D, Wang F, Chen T, Chen WR. 2007. Mechanistic study of apoptosis induced by high-fluence low-power laser irradiation using fluorescence imaging techniques. J Biomed Opt 12:064015.
Wu S, Xing D, Gao X, Chen WR. 2009. High fluence low-power laser irradiation induces mitochondrial permeability transition mediated by reactive oxygen species. J Cell Physiol 218:603–611.
Yamada T, Katagiri H, Asano T, Inukai K, Tsuru M, Kodama T, Kikuchi M, Oka Y. 2001. 3-Phosphoinositide-dependent protein kinase 1, an Akt1 kinase, is involved in dephosphorylation of Thr-308 of Akt1 in Chinese hamster ovary cells. J Biol Chem 276:5339–5345.
Yang L, Sun M, Sun XM, Cheng GZ, Nicosia SV, Cheng JQ. 2007. Akt attenuation of the serine protease activity of HtrA2/Omi through phosphorylation of serine 212. J Biol Chem 282:10981–10987.
Zhang J, Xing D, Gao X. 2008. Low-power laser irradiation activates Src tyrosine kinase through reactive oxygen species-mediated signaling pathway. J Cell Physiol 217:518–528.
Zhang L, Xing D, Gao X, Wu S. 2009. Low-power laser irradiation promotes cell proliferation by activating PI3K/Akt pathway. J Cell Physiol 219:553–562.
Zhang L, Zhang Y, Xing D. 2010. LPLI Inhibits apoptosis upstream of Bax translocation via a GSK-3β-inactivation mechanism. J Cell Physiol 224:218–228.